Quartz Crystal Microbalance Application for Characterization of Nanomaterials In Situ

10

Victor S. Popov and Alexander Sopilniak

Contents

Abbreviations

AFM	Atomic Force Microscopy
CVD	Chemical Vapor Deposition
EQCM	Electrochemical Quartz Crystal Microbalance
GO	Graphene Oxide
IR	Infrared
MWCNT	Multiwalled Carbon Nano Tubes

V. S. Popov (✉)
Department of advanced research and development, Polyus Research Institute of M.F.Stelmakh, Moscow, Russia

Sector for high-temperature and sensor materials, Kurnakov Institute of General and Inorganic Chemistry, The Russian Academy of Sciences, Moscow, Russia
e-mail: popov.chem@gmail.com

A. Sopilniak
The Institute of Chemistry, The Hebrew University of Jerusalem, Jerusalem, Israel

C. S. S. R. Kumar (ed.), *In-situ Characterization Techniques for Nanomaterials*,
https://doi.org/10.1007/978-3-662-56322-9_10

NOM	Natural Organic Matter
NP	Nanoparticle
NR	Nanorod
NS	Nanospheres
NW	Nanowires
PVD	Physical Vapor Deposition
QCM	Quartz Crystal Microbalance
QCM-D	Quartz Crystal Microbalance with Dissipation Monitoring
QCR	Quartz Crystal Resonator
QD	Quantum Dot
QMB	Quartz Microbalance
SAM	Self-Assembled Monolayers
SEM	Scanning Electron Microscopy
SPM	Scanning Probe Microscopy
STM	Scanning Tunneling Microscope
SWCNT	Single-Walled Carbon Nano Tubes
TEM	Transmission Electron Microscopy

1 Definition of the Topic

Quartz crystal microbalance (QCM) or quartz microbalance (QMB) as an in situ precise method for mass control allows vast research of many processes of heterophasic mass transfer.

In the current chapter, we discuss the recent research dedicated to the application of QCM to study growth and degradation processes of nanomaterials, as well as interactions of nanomaterials with different compounds and natural systems, including compounds from a biological origin.

2 Overview

It is a common conception that the era of nanoscience began with the development of a measurement device, giving the necessary resolution to identify a nano-object – the scanning tunneling microscope or STM. The development of a high resolution both scanning and transmission electronic microscopy (SEM and TEM, respectively) quickly followed the STM development and surpassed its abilities to receive a clear image of nano-objects. The SEM/TEM images were highly detailed and opened the possibility to study substructures and crystal structures of the objects. The development of new research tools led to the discovery of nano-scale phenomena, which, in turn, explained the unique properties of well-known materials. The systematic study of the reasons behind the appearance of nano-scale phenomena could have been achieved only with the development of specialized tools and precise methods of analytical quantification.

Quartz crystal microbalance (QCM) or quartz microbalance (QMB) as a measurement tool could monitor changes in mass on the scale of nano to pico grams in real time as well as registering precise changes in viscoelastic properties and structures of materials on thin films, even in cases where such accuracy cannot be achieved with atomic force microscopy. It is therefore a highly necessary and desired research tool in the study of nanomaterials.

Here, we look at the application of QCM for the study of processes related to the growth and degradation of nanostructures and ultrathin films, and the detection of molecular analytes by sensor-nanomaterials and nanoparticle-analytes on specialized receptors. Moreover, a large portion of this work is dedicated to the application of QCM in research of nanostructures transport in different ecosystems as well as nanomaterial toxicology.

3 Introduction

The piezoelectric effect is the occurrence of an electrical potential on certain materials due to mechanical deformation (e.g., quartz). The effect was first discovered in 1880 by Paul-Jacques and Pierre Curie [1]. A year later in 1881, a reverse effect was hypothesized by Lippman [2], which was experimentally proven by the Curie brothers later on that year [3]. Nevertheless, the mathematical analysis, connecting the reverse piezoelectric effect with the changes in a resonator's mass, appeared only 77 years later in the work of Sauerbrey [4]. The proposed method allowed conducting measurements of changes in a resonator's mass with very high sensitivity, which was limited only by the nature of the quartz crystal, used for this purpose. The later was the basis of the development of the quartz crystal microbalance (QCM). Modern day piezoelectric quartz crystal resonators (QCR) can detect changes in mass on the scale of 10^{-9}–10^{-12} grams. A disadvantage of the method is the relatively narrow range of measurement.

Due to the high precision and sensitivity, QCM was widely used for different applications: (a) for quality control of layer depositions, to allow evaluating the thickness of the deposited layer; (b) for piezoelectric mass sensors armed with layers of receptors, ensuring selective binding of an analyte; (c) for research purposes of investigating in situ processes of deposition and growth of layers.

The rapid development of nanoscience and nanotechnology in the last decade of the twentieth century renewed the interest of the scientific community in QCM. Foremost, it became apparent that QCM is irreplaceable as an instrument of in situ measurements of thin layer thickness in electronics in both chemical and physical vapor deposition (CVD and PVD, respectively) apparatus [5], even with recent developments in process technology (14–10 nm) [6]. Moreover, it is possible to utilize QCM not only for layer thickness control but also for the studies of nanomaterial growth and aggregation from both gas and liquid phases [7].

Work in the field of nanomaterials introduced the concept of nanomaterials as receptor layers on piezoelectric mass sensors [8, 9].

Finally, as nanomaterials were incorporated into the industry, scientific attention was devoted to questions regarding the influence of these materials on living organisms and the environment, leading to new branches of nanoscience "nanopharmacology" and "nanotoxicology" [10]. For these reasons, QCM became a vital instrument for investigation of interaction processes of nanoparticles with various biomolecules, development of analytical methods for biosensing of and with nanomaterials [11, 12], as well as in biotechnology [13] and toxicology [14].

As a traditional instrument for mass-metric process control, QCM was utilized not only as a research tool but is also utilized for educational purposes. For example, process control of self-assembled monolayers (SAMs) using QCM was suggested in a paper from Cea et al. [15] as an educational experimental work for students of nanoscience and nanomaterials.

The questions of application of QCM were partially discussed in previously published reviews, covering only a narrow spectrum of nanoscience and nanotechnology, for instance, nanosensors and analytics [12, 16–18] or nanomedicine and health care [19–21]. However, no specialized review covers broad practical applications of QCM in the field of nanoscience.

The latest tightly themed review was published in 2016 and focused on the application of QCM in the research of nanoparticle interactions, with emphasis of aggregation and deposition on nanoparticles from colloidal solutions [22]. The authors devoted much attention to the type of works described by the DLVO theory (Derjaguin, Landau, Verwey, and Overbeek theory). During the course of discussing the forces governing the aggregation process, the authors present research works in application of QCM for investigating only aggregation and deposition processes from colloidal solutions, but for different nano-objects (carbon-based, metal, metal oxide and other nanoparticles).

The goal of the present work is to conduct a systematic review, for the first time, of all possible directions of QCM application in the research of nano-objects. This review includes original publications from the last 6 years. A detailed inquiry using databases such as Web of Knowledge and CAS revealed advancements in the application of QCM. Noticeable work was observed in the following directions: nanomaterial-based sensors, nanotoxicology, detection of nanoparticles as analytes, research of ecological aspects of nanoparticle transportation and distribution in the environment, the study of growth and formation of nanostructures during nanomaterial synthesis, and different and unusual applications of QCM for process control of nanostructures deformation because of external influence. Moreover, this review includes studies dedicated to the combinations of QCM with other methodologies for a better in situ characterization of the investigated processes.

Based on the current review of the latest research trends using QCM at their center, the expansion perspectives of QCM and QCM combined methods application for the study of nanostructures were discussed in the concluding section of this chapter.

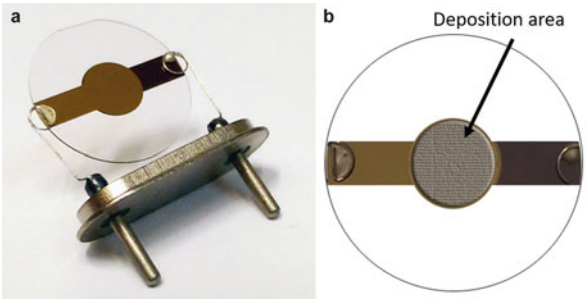

Fig. 10.1 Quartz crystal resonator in holder (**a**) and scheme of deposition area on frontal electrode (**b**)

4 Experimental and Instrumental Methodology

4.1 Working Principle

The core of any quartz microbalance is the piezoelectric quartz crystal (usually with an AT cut) with two adjacent metal electrodes (Au, Pt, Ag), together referred to as the quartz crystal resonator (QCR). Due to the reverse piezoelectric effect, when electrical potential is applied between the two electrodes, the quartz crystal begins to resonate. The frequency of resonance is an internal property of the crystal, as well as all the higher resonance harmonics. The value of the resonance frequency tightly depends on the mass of the crystal (Fig. 10.1).

Relationship between the change of the QCM frequency and the change of the mass can be found from the Sauerbrey model [4]:

$$\Delta f = 2.3 \cdot 10^6 \cdot F_0^2 \cdot \frac{\Delta m}{s} \tag{10.1}$$

where Δf – change the oscillation frequency of quartz resonator at the fundamental harmonic, Hz; F_0 – the natural vibration frequency of the QCR, in MHz; Δm – mass change of the QCR, in gr; s – area of the oscillating part of the QCR (between contacts), in cm^2.

Substitution in (1) the specified values (i.e., F_0, s *and* ΔF) allow to estimate the change of the sample mass as a function of the change in frequency for the first harmonics of quartz crystal:

$$\Delta m = -C\mathrm{m} \cdot \Delta f \tag{10.2}$$

or for harmonics number n [23]:

$$\Delta m = -C\mathrm{m} \cdot \frac{\Delta f}{n} \tag{10.3}$$

where C_m is a constant of the resonator parameters from Eq. 10.1.

The Sauerbrey model gives an accurate description for the cases of deposition for a gas phase or for vacuum, and only for thin rigid films.

For cases of nonrigid films, the Sauerbrey model cannot be applied. These cases use an additional measurement of dissipation energy, which describes the scattering rate of the resonance energy of the crystal to the surroundings. When any material is applied on the QCR surface, the dissipation energy will correlate with the viscoelastic properties of the material. High viscoelastic materials will better dissipate the resonance energy.

The dissipation energy can be evaluated from the dissipation factor D, which can be estimated as follows [24]:

$$D = \frac{1}{\pi F \tau} \tag{10.4}$$

where F is the resonance frequency and τ – decay time constant.

Most cases use the Voigt-based model, described in Eqs. 10.5 and 10.6 [23, 25], which correlates between the density and length of the quartz crystal (ρ_q and h_q), characteristics of the adsorbed film or coating material (h_f – thickness, μ_f – elastic modulus, η_f – viscosity, ρ_f – density), and the bulk-liquid density and viscosity (η_l and ρ_l).

$$\Delta F = \mathrm{Im}\left(\frac{\beta}{2\pi\rho_q h_q}\right) \tag{10.5}$$

$$\Delta D = -\mathrm{Re}\left(\frac{\beta}{2\pi F\rho_q h_q}\right) \tag{10.6}$$

where

$$\beta = \xi_1 \frac{2\pi F\eta_f - i\mu_f}{2\pi F} \frac{1-\alpha e^{2\xi_1 h_f}}{1+\alpha e^{2\xi_1 h_f}},$$

$$\alpha = \frac{\frac{\xi_1}{\xi_2}\frac{2\pi F\eta_f - i\mu_f}{2\pi F\eta_l} + 1}{\frac{\xi_1}{\xi_2}\frac{2\pi F\eta_f - i\mu_f}{2\pi F\eta_l} - 1},$$

$$\xi_1 = \sqrt{-\frac{(2\pi F)^2\rho_f}{\mu_f + i2\pi\eta_f}},$$

$$\xi_2 = \sqrt{i\frac{2\pi F\rho_l}{\eta_l}}.$$

For some cases described in this review, a nonrigid film is formed, especially for deposition from a liquid phase; the full Voigt-based model can be used. However for practical reasons, the signal analysis is limited to measurements of the changes in frequency and dissipation without additional description.

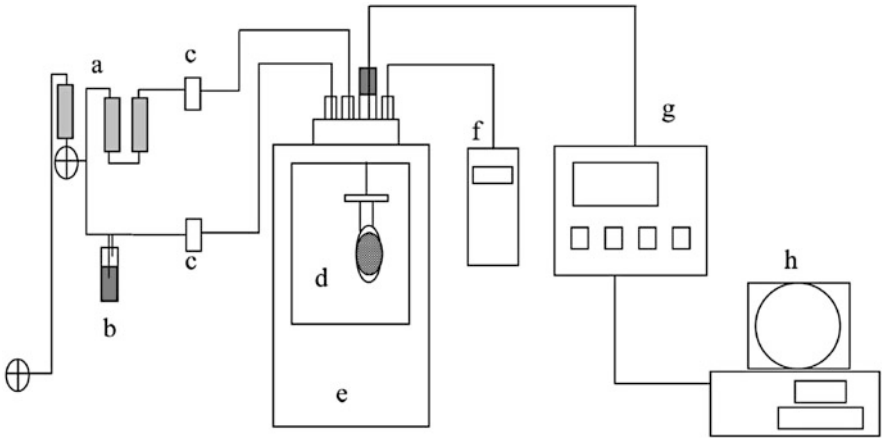

Fig. 10.2 Schematic diagram of experimental setup for the QCM sensor measurement and low humidity atmosphere controller. (**a**) Molecular sieve and desiccating agent; (**b**) water; (**c**) mass flow controller; (**d**) detecting chamber and QCM; (**e**) thermostat; (**f**) low humidity hygrometer; (**g**) oscillator and frequency counter; (**h**) PC [26]

4.2 Tools for Research

4.2.1 Quartz Crystal Microbalance with Dissipation Monitoring (QCM-D)

Quartz crystal microbalance with dissipation monitoring (QCM-D) is the most common and used commercial version of QCM. QCM-D has a hermetic gas/liquid chamber, which can be used for flow experiments. The chamber contains the QCR holder, connecting the electrodes to an electrical circuit (Fig. 10.2). When a QCR sits in the measurement chamber, it is connected to an oscillator and frequency counter. The mass flow controller (Fig. 10.2c), which introduces the gas/liquid sample into the chamber, is connected to the entrance of the detecting chamber (Fig. 10.2d). QCM-D can also be equipped with a thermostat and a humidity hygrometer (Fig. 10.2e–f). QCM can come without the dissipation monitoring system, but the difference between them is in an additional computation block.

4.2.2 In Situ Electrochemical Quartz Crystal Microbalance (EQCM)

In situ electrochemical quartz crystal microbalance (EQCM) is similar in construction to QCM-D with additional electrochemical components in the detecting chamber. The EQCM measuring chamber is integrated with a counter and a reference electrode. The working electrode is the QCR (Fig. 10.3). The electrodes are connected to a potentiostat.

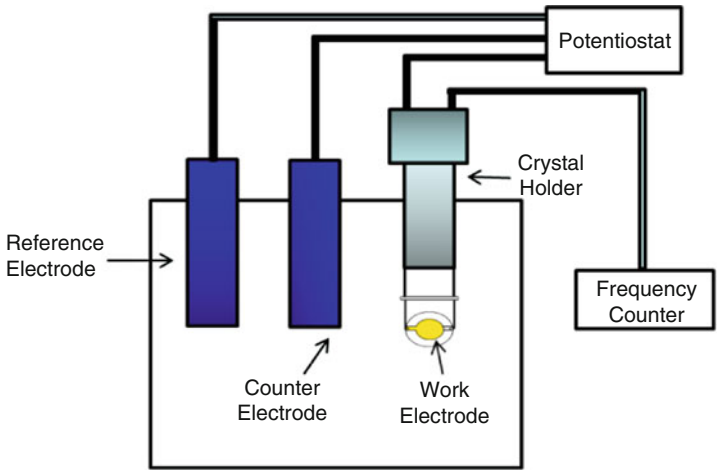

Fig. 10.3 In situ electrochemical quartz crystal microbalance (EQCM) [27]

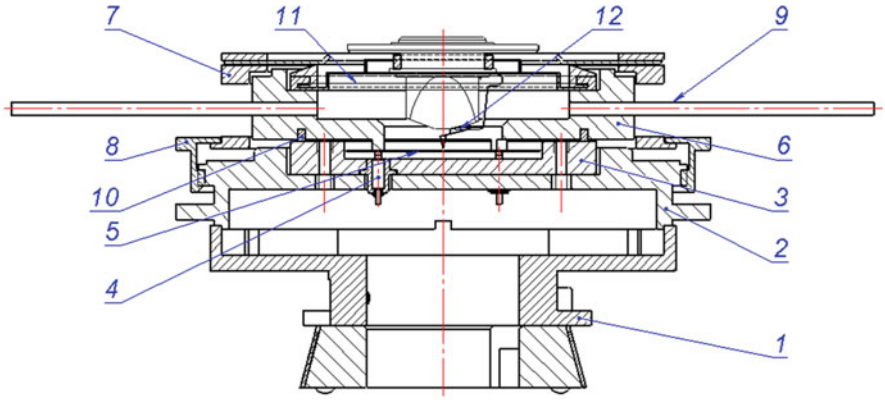

Fig. 10.4 Gas-liquid cell with integrated quartz microbalance [28]

4.2.3 Integrated System Scanning Probe Microscope: Quartz Microbalance

Figure 10.4 shows the design of the gas-liquid cell for an integrated system scanning probe microscope – quartz microbalance: in situ testing of surface potential, topography, and mass of the adsorbed gases [28, 29]. The cell consists of a carriage (1), base (2), bottom cell part (3) with a build-in gold-coated spring contacts (4). Quartz-crystal resonator (QCR) (5) is placed on spring contacts. Fixation of the QCR is carried out by a top cell part (6) with a nozzle (7) and by a screw-nut (8). The gas is supplied through input/output connectors (9). Tightness of the cell is provided by an O-ring (10) between the upper and lower part, and a rubber membrane (11) between

the probe holder and the upper part. An AFM probe (12) is fixed in the probe holder, which allows you to apply electric AC/DC voltage to the probe.

5 Key Research Findings from the Review

5.1 Application of QCM in Studying Nanomaterials for Sensors

Nanomaterials have large surface areas, hence a large number of active centers, which in turn, allow their very broad application as catalysts and highly selective materials for sensors in the gas and liquid phases. Recent works showed promising developments in utilizing nanomaterials as receptors or as matrix for receptor materials for mass sensitive sensors. Recently, carbon nanostructures, such as multiwall carbon nanotubes (MWCNT), MWCNT-COOH (carboxyl functional group), and graphene oxide (GO), were used as receptor materials for sensing water vapor via sorption onto their surface [26]. QCM was used as means to assess the sorption rate and efficiency through measurements of changes in mass. The studied water vapor concentrations were as low as 345 ppm. The authors demonstrated a correlation between the number of functional groups on the surface of MWCNT-COOH and GO (determined using IR spectra) and the sensitivity for low water vapor concentrations. The highest sensitivity to water vapor concentrations was shown for GO based on observations of a larger sorption rate and association constants of water vapor than the corresponding constants for MWCNT-COOH. The authors attribute the difference in sensitivities to the number of -COOH groups on the surface of these materials.

In a paper by Barsan et al. [30], a graphene-based receptor is used as an enzyme biosensor. The activity of the system was demonstrated using QCM as a sensing device for accumulated enzyme (layer deposition). The authors show a rise in deposition of layer containing glucose oxidase enzymes onto the surface of the gold QCM electrode in the presence of nitrogen-doped graphene, used as a template for immobilization of enzymes. The use of nitrogen-doped graphene was shown to increase the sensitivity of the biosensor. Further research is suggested for different nanostructures such as carbon nanotubes/nanorods and fullerenes.

The application of nanostructures as a matrix for receptor materials was successfully shown for a previously developed aptasensor by Du et al. [31]. The binding of microcystin-LR (MC-LR) with the electrochemiluminescence aptasensor, based on three-dimensional boron and nitrogen codoped graphene hydrogels (BN-GHs), was registered using QCM (Fig. 10.5). BN-GHs were applied on a QCR and change in mass was registered due to the binding of the model selective target.

In an interesting research effort, the combination of several in situ techniques, which allow the study of material sensor properties, was proposed by Popov et al. [28]. This idea was demonstrated using a device, integrating both QCM and a scanning probe microscope (SPM), for in situ detection of gas sorption properties on surfaces of nanostructures (Fig. 10.4). Different materials were applied on gold electrode quartz resonators (QCR): SnO_2, palladium-doped tin dioxide (SnO_2-Pd),

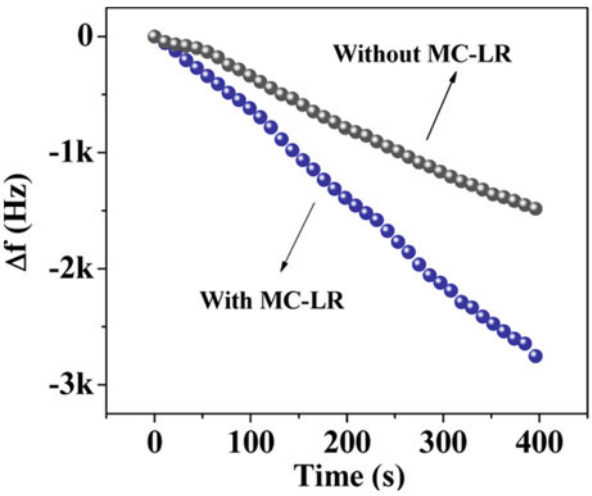

Fig. 10.5 Frequency responses of the aptamer-based QCM biosensor without and with being incubated with 5 pM MC-LR [31]

Table 10.1 Response of QCM and the Kelvin probe at the action of analytes [28]

Sample	Change of the vibration frequency of resonator, Hz (change in the mass, calculated by the Sauerbrey model, ng)			Change of the average surface potential of samples, mV		
	10% (vol) NH_3 in air	0.1% (vol) H_2 in air	0.1% (vol) CH_4 in air	10% (vol) NH_3 in air	0.1% (vol) H_2 in air	0.1% (vol) CH_4 in air
SnO_2	758(2198.2)	420(1218.0)	38(110.2)	189.0	54.7	68.9
SnO_2-Pd	115(333.5)	<1 (−)	70(203.0)	25.8	22.5	30.0
BCP-HfO_2	15(43.5)	1(2.9)	1(2.9)	6.6	15.7	14.1
QCR	12(8.7)	<1(−)	<1(−)	46.3	13.5	6.4

and hafnium dioxide coated with bromocresol purple (HfO_2– BCP). The analyte gases (NH_3, H_2, and CH_4 mixtures with air) were introduced into the measurement chamber, containing one of the nanostructures. Due to gas sorption, frequency shifts were registered with QCM and changes in surface potential were mapped with SPM using a Kelvin probe over an area of 100 × 100 nm. The results are summarized in Table 10.1. These results suggest that sensor properties can be assessed using a single nanocrystal with a surface area of 10^{-8} mm^2.

5.2 Application of QCM for Nanotoxicology and Detection of Nanomaterials as Analytes

The large investment in nanotechnology in the last two decades triggered rapid development of the field of nanoscience and the use of nanomaterials as common analytes. Due to the small scale and high permeability of nanostructures, research effort was devoted to the newly raised question of toxicity of nanomaterials for

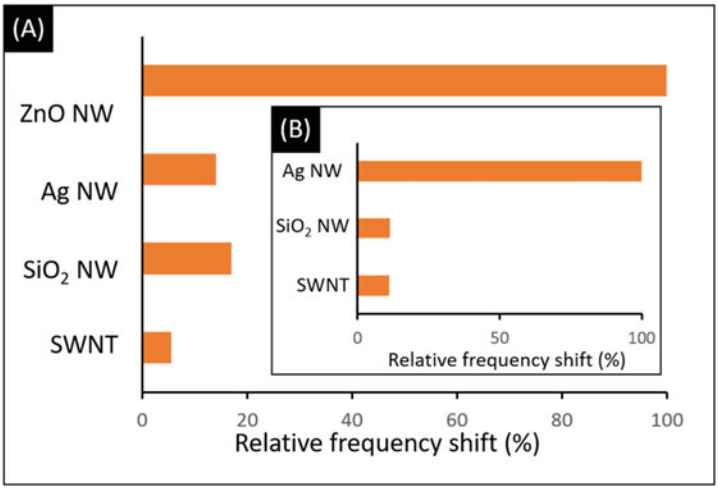

Fig. 10.6 (**a**) Relative frequency shifts for Ag NW, SiO_2 NW, and SWCNT in comparison with ZnO NW; (**b**) relative frequency shifts for SWCNTs and SiO_2 NWs in comparison with Ag NWs. Plot based on data [33, 34], respectively

living organisms. The forecast of size of the global market for nanotoxicology by the year 2019 is expected to reach 64.2 billion dollars [32]. In the last few years, many methods were developed not only for characterizing the toxicity of nanostructures but also for detection of nanostructures as toxic agents, including methods based on QCM.

5.2.1 Application of QCM in Sensor Systems for Detection of Nanomaterials as Analytes

Among the vast number of investigated nanostructures, nano-ZnOs are especially interesting, due to their semiconductive and piezoelectric properties. Jang et al. [33] depicts a method for detection of zinc oxide nanowires (ZnO NWs) based on the covalent interaction between the nanowires, modified with a single-stranded DNA (i.e., linker DNA) using a phosphoric acid group, and the QCM electrode surface, modified with single-stranded DNA containing thiol groups. The authors report a sensitivity level that is 105 times higher than the toxic ZnO NW concentration level in deionized water (limit of detection of 10^{-4} μg/ml).

It should be noted that this method of detection has rather long response times (90% of sensor saturation). For concentrations between 100 pg/mL and 10 ng/mL, as well as for 10 μg/mL, the reported response time was between 10 and 25 min, while for the mid-range concentrations of 100 ng/mL–1 μg/mL, the response time reached 45–50 min.

Other commonly used inorganic materials were also detected using the suggested method (AgNW, SiO_2NW, and single-walled carbon nanotubes (SWCNTs)), and their relative sensitivity compared to ZnO NW detection is depicted in Fig. 10.6a. The low sensitivity to inorganic materials was explained by the absence of interactions with the DNA or by interaction resulting in a low mass difference.

However, a following paper by the same authors reports contradicting results, suggesting high sensitivity for Ag NW in an analogous method, which makes use of the same modifications for NW as well as for the QCM electrodes (Fig. 10.6b) [34]. In 2015, another paper by Jang et al. was released, in which the same methodology was successfully applied for detection of SWCNTs [35].

Unfortunately, the authors did not conduct comparison analysis between their works. Therefore, the selectivity of the suggested method remains to be determined in further research efforts.

5.2.2 Using QCM for Nanotoxicology Research

Developments in the field of nanomedicine increase the human exposure to nanomaterials in the forms of diagnostic and therapeutic agents [36]. Recent QCM-based studies explore the effects of nanostructures on the human body.

The effects of CdTe quantum dots (QD) on the functionality of human blood platelets were demonstrated by Samuel et al. [37] using a QCM-D device. In the course of the study, the QCR was coated with fibrinogen (plasma protein). The changes in frequencies and dissipation response due to platelet deposition were monitored as the QCR was placed in contact with platelet rich plasma (PRP) and platelet poor plasma (PPP) in the presence and absence of CdTe QDs. Measurements were carried out in the third harmonic. The authors did not observe any influence of the CdTe QDs on the deposition of platelets for PPP; however, for PRP, CdTe QDs increased the deposition by 25% due to platelet aggregation. The QCM was reported to be more sensitive to the influence of QDs on the aggregation of platelets than for the commonly used method in such cases, light transmission aggregometry (LTA).

A positive effect to toxicity of nanomaterials was found in a study dedicated to the aggregation of amyloid beta (Aβ) peptides, which cause the amyloid plaques in the brain associated with Alzheimer's disease. The aggregation inhibition with graphene was investigated by Jie Wang et al. [38]. The effects of GO sizes on Aβ (33–42) peptide aggregation were monitored. The shifts in frequencies of a quartz resonator were registered due to precipitation on the surface of its gold electrodes. Various solutions were used with combinations of different GO sizes and Aβ (33–42) peptide (amino acid sequence: NH_2-GLMVGGVVIA-COOH). This experiment illustrates the enhancement of inhibition of Aβ (33–42) peptide aggregation with increasing GO size. These results can become a basis of a new specific inhibition technique for Aβ (33–42) peptide aggregation. Nevertheless, this approach requires additional research on the other effects of GO on a living organism, for instance, toxicity to other proteins.

Toxic effects of deposition of multiwalled carbon nanotubes (MWCNTs) on biological membranes were checked as a function of electrolyte concentration, cation charge, and solution pH [39]. Supported lipid bilayers (SLBs) composed of zwitterionic 1,2-dioleoyl-sn-glyero-3-phosphocholine (DOPC) and vesicles were used as model biological membranes. QCRs were coated with SLBs and vesicles by the method described in Richter et al. [40]. The system was put in different solutions containing the model membranes. The authors show favorable deposition of MWCNTs on biological membranes in acidic conditions (pH 2–3) as well as in the presence of Ca^{2+} ions (Fig. 10.7).

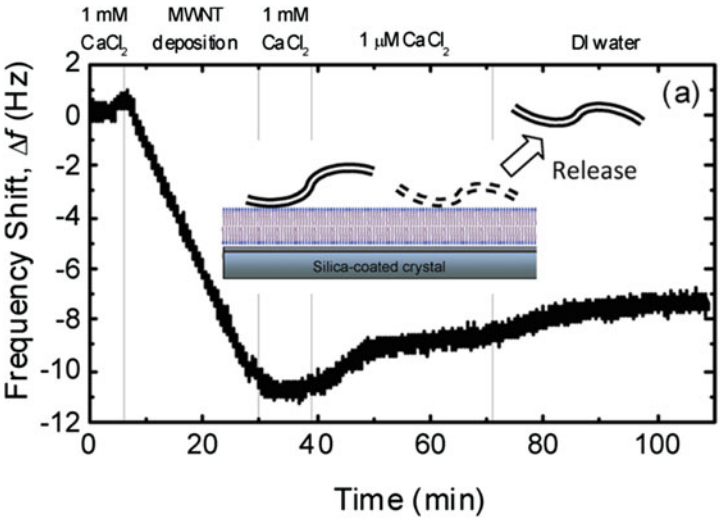

Fig. 10.7 Frequency (blue) and dissipation (red) shifts during the formation of a supported vesicular layer (SVL) and the deposition of MWCNTs on the SVL at 1 mM $CaCl_2$ and pH 7.3. The inset illustrates the deposition of MWCNTs on a SVL (not drawn to scale) [39]

The reversibility of deposition was also observed when rinsing the membranes with low ionic strength solutions at slightly basic conditions (pH 7.3). In addition, a study of the interactions between graphene oxide (GO) sheets of different sizes and small and large liposomes prepared from 1-palmitoyl-2-oleyl-*sn*-glycero-3-phosphocholine (POPC) and 1-palmitoyl-2-oleyl-*sn*-glycero-3-ethyl- phosphocholine (POEPC) [41]. On the surface of a QCR, a layered structure was constructed in the following order: liposomes, GO, small and large unilamellar vesicles (SUVs and LUVs), and GO. QCM-D was used to monitor both frequency shifts (ΔF) due to material adsorption and shifts in dissipation (energy, ΔD). The ΔD-response serves as an indication of viscoelastic coating properties on the QCR. As a result, the lateral dimensions of liposomes and GO were obtained. ΔF and ΔD together allowed the construction of a schematic representation of the process (Fig. 10.8).

Implant integration in the body (soft tissue and osseointegration) can possibly be improved by coating the implant surface with different nanoparticles. In a recent study, the adhesion properties of human gingival fibroblasts were tested on the surface of hydroxyapatite and titanium nanostructures using QCM-D, as materials of interest for dental implant applications [42]. Titanium and hydroxyapatite nanostructures (nanoHA) coated titanium crystals were applied on a surface of a quartz resonator. The authors used a cell suspension, which was introduced into the QCM-D measurement chamber with a constant flow rate. Simultaneously, the adhesion and cell coverage kinetics of the cells were observed in situ while registering shifts in frequencies and dissipation of the resonator. Interestingly, no difference was found in cell spreading rate on titanium and nanoHA, and further studies are advised in order to conclude whether nanoHA and titanium improve soft tissue integration or not.

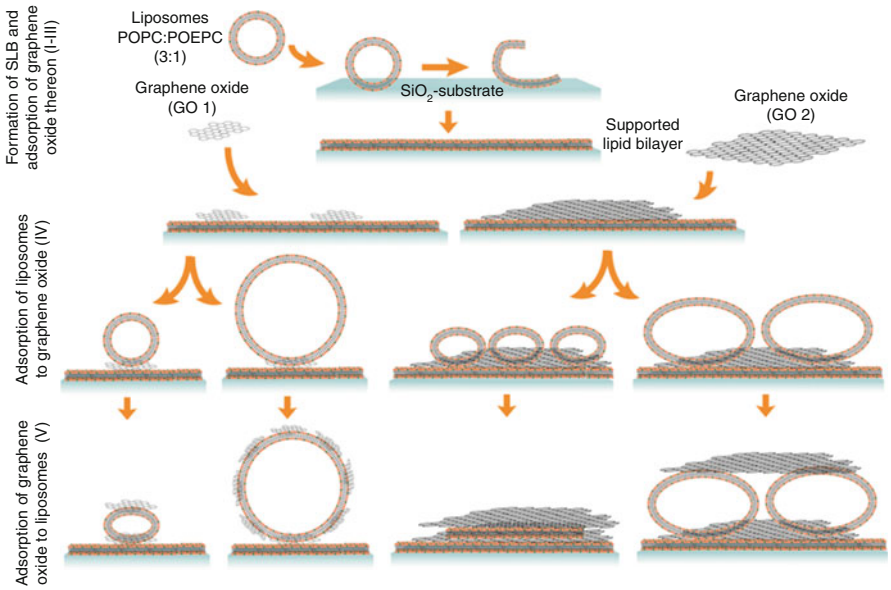

Fig. 10.8 Schematic representation of the GO/lipid membrane (SLB and liposome) interactions, deduced from the data presented in Fig 2.2. The following series of events is illustrated (from the top): (I) addition of liposomes, (II) spontaneous formation of a supported lipid membrane, (III) addition of GO 1 (90 nm) and GO 2 (500–5000 nm, GO sheet sizes in the lower end of this range are dominating), (IV) addition of SUVs and LUVs to adsorbed GO 1 and GO 2, and (V) addition of GO 1 and GO 2 to the adsorbed liposomes. Not drawn to scale [41]

A mechanistic understanding of nanoparticle-induced bacterial toxicity has implications for understanding ecosystem health in general. *Shewanella oneidensis* (metal-reducing bacteria) were chosen as a model system for understanding nanotoxicity (due to their importance for geochemical nutrient cycling) in a study of the influence of TiO_2 nanoparticles on biofilm formation and riboflavin secretion using QCM [43]. In an incubator of 30 °C, a QCR was immersed into a Lysogeny broth (LB), followed by a suspension of bacteria and clean LB. TiO_2 nanoparticles were introduced with the LB or bacteria. The authors used nanoparticles of three kinds: self-synthetized and commercial P25 and T-Eco nanoparticles. The different nanoparticles were used to differentiate between the effects of mass changes due to deposition and biofilm growth. The authors show a decrease in biofilm formation rate in the presence of TiO_2 nanoparticles. Interestingly, riboflavin secretion was increased significantly as a function of present nanoparticles (Fig. 10.9). Both phenomena were attributed to cellular stress response.

5.3 QCM for Study of Environmental Aspects of Nanomaterials

Incorporation of structural and functional nanomaterials in industrial production is a competitive advancement with a substantial profit for any company. This fact let to

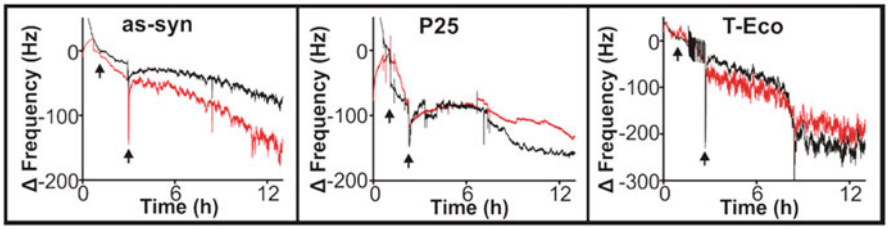

Fig. 10.9 QCM analysis of bacteria exposed to 25 μg/mL as-syn, P25, or T-Eco nanoparticles during bacterial attachment, indicated by the window of time between the arrows. Red = TiO2 exposure and black = control (no nanoparticles) introduced in LB broth [43]

worldwide distribution of products containing nanostructures. Nevertheless, in many cases the producing company does not take under consideration the ecological aspects regarding the effects of nanomaterial on the environment. Therefore, in the last two decades, research in environmental science has become vaster. Not only for the study of toxicity of nanomaterials of living organisms but also for the study of distribution, transport, adsorption, and accumulation as well as biodegradation in the environment. Among the most commonly used nanomaterials in industry, two main groups stand out due to their chemical nature: metal nanoparticles and their binary compounds, including quantum dots, and another large group is the different nanoforms of carbon, such as fullerene, carbon nanotubes, graphene and its derivatives.

5.3.1 Nanoparticles of Metals and Metal Compounds

In a recent paper by Afrooz et al. [44], the influence of the shape of nanoparticles on the nature of aggregation and deposition was studied using QCM with an emphasis on aquatic ecosystems. The authors used gold nanospheres (AuNSs) and nanorods (AuNRs) coated with polyacrylic acid (PAA) as model nanostructures. The deposition rate of the nanoparticles onto a silica-coated quartz crystal was measured using in NaCl solution of concentrations between 10 and 1000 mM (Fig. 10.10). The authors show an increase in deposition rate with increased electrolyte concentration. The observed differences in deposition rates are attributed in the article to unique packing of the nanoparticles as well as to various chemical interfacial properties. In a similar study, Quevedo et al. [45] utilized QCM to study the deposition of commercial quantum dots (QDs) on the surface of Al_2O_3, which is present on aquifer or filter grain, and in the presence of dissolved organic molecules (DOM). CdTe/CdS QDs were stabilized with polyacrylic-acid (PAA) and CdSe/ZnS QDs were coated with poly-ethylene-glycol (PEG) in the form of water suspensions. Carboxyl-functionalized (cPL) and sulfate-functionalized (sPL) polystyrene latex nanospheres were used as control samples.

The model DOMs used were Suwannee River humic acid (SRHA) and JBR215 (10% mixture of the two rhamnolipids RLL ($C_{26}H_{48}O_9$) and RRLL ($C_{32}H_{58}O_{13}$)) as coating material as well as for QD suspension preparation. The alumina-coated QCR was put first in electrolyte-rich solutions (KCl) and afterward in the QD suspensions. Measurements with QCM showed the deposition rate decreases with the increase in

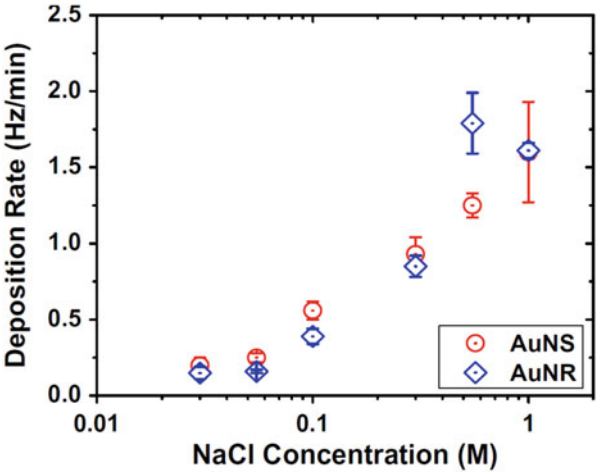

Fig. 10.10 Deposition rates of AuNPs onto a silica-coated quartz crystal in the presence of NaCl. Deposition rates are expressed as the rates of normalized frequency shift at the third overtone. Each data point represents the mean of triplicate measurements conducted at the same experimental conditions, and the error bars represent standard deviations. Measurements were carried out at 20 °C [44]

occupied surface area. The maximum deposition rate was observed in the first minute. The authors note that the deposition rate is affected by modifications of the surface of the QDs and the composition of their solution (Fig. 10.11). The surface-modified QDs had a lower deposition rate on the Al_2O_3 than the model polymer nanoparticles. Coating Al_2O_3 with DOM adds an additional electrostatic barrier (due to charge reversal), which decreases the retention of all QDs. Hence, the deposition of charged QDs is not favorable on adsorbing materials containing DOM in natural systems and filters.

5.3.2 Carbon Nanoforms

The fate and distribution of fullerene C60 in natural systems peaks research interest due to their potential risk to the natural ecosystem and human health. In a study by Tong et al. [46], the influence of biofilms on the transport of fullerene (C60) nanoparticles was studied both using QCM and in soil-like porous media. The biofilms were encapsulated in extracellular polymeric substances (EPS), which was extracted from *E. coli*. QCR with precoated silica surfaces or with EPS was put in solutions of C60 and NaCl, $CaCl_2$ with different environmentally relevant concentrations. Measurements were carried out in a flow system. The authors report that an increased deposition of C60 is observed probably due to the increase in the roughness of SiO_2 in the presence of a biofilm (Fig. 10.12). Hence, biofilms can assist in the inhibition distribution and transport of C60-like materials in the natural ecosystems.

In a parallel study, the thermal dependence of fullerene C60 on the surface of SiO_2 was investigated in the presence and absence of Harpeth humic acids and Harpeth fulvic acids (HHA and HFA), representing the dominant organic components in soils and sediments (soil organic matter (SOM) and attached phase soil organic matter (AP-SOM)) [46].

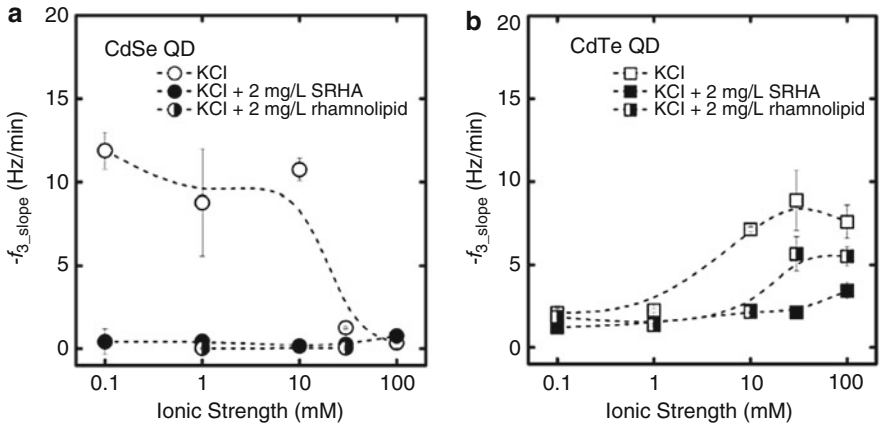

Fig. 10.11 Deposition rates of the QDs over a range of ionic strength (pH 5) onto DOM precoated Al_2O_3 (i.e., SRHA, rhamnolipid) and bare Al_2O_3. The different solution chemistries are represented with full symbols for KCl supplemented with 2 mg/L SRHA, half full symbols for KCl with 2 mg/L rhamnolipid, and open symbols for simple KCl. Data represent the mean ± standard deviation [45]

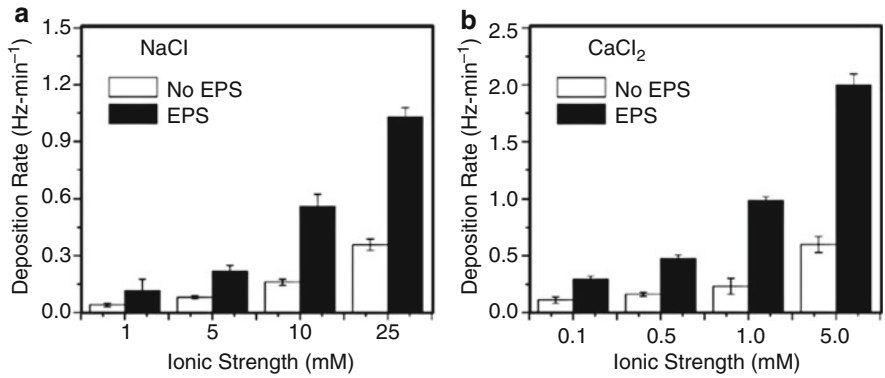

Fig. 10.12 Deposition rate (k_f) of fullerene C60 on bare (white bar) and EPS-coated silica surface (black bar) in NaCl (top) and $CaCl_2$ (bottom) solutions at pH 6.8 (adjusted with 0.1 M NaOH) as a function of ionic strength in QCM-D. Duplicate measurements were conducted over entire ionic strength range, with error bars representing standard deviations [46]

The working electrode of a QCM quartz resonator was used as a model surface. The electrodes were coated with a layer of SiO_2. The study shows a rise in interactions of C60 with immobilized HHA and HFA at higher temperatures, while the interactions with the clean surface of SiO_2 were mostly independent of changes in temperature (Fig. 10.13). The authors attribute this behavior to water-assisted disruption of polar SOM contacts and hydration-induced swelling of AP-SOM matrix. Structures such as C60 are predicted to accumulate in soil and sediments during warm seasons. Further research in this field will be able to predict more

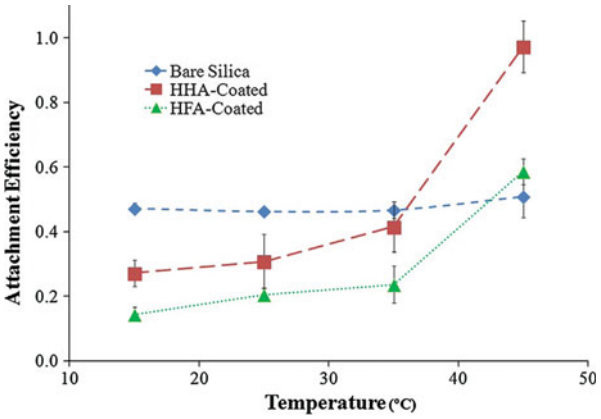

Fig. 10.13 C60 attachment efficiencies onto bare, HHA-coated, and HFA-coated silica sensors as a function of temperature. Error bars represent the standard deviation [47]

accurately the possible anthropological effects on similar ecosystems and to develop the means to counter negative interactions of this sort. A following work by the same authors demonstrated the use of QCM for the study of deposition kinetics of colloidal fullerene C60 particles (nC60) as a result of interaction with HHA in the presence of various electrolyte concentrations [48]. A SiO_2-coated QCR was put into electrolyte solutions with different concentrations and HHA. After reaching equilibrium, the nC60 solution was introduced into the setup. The slope of the linear section in Fig. 10.14f corresponds to the deposition rate (Hz/min) of nC60 onto the surface of the resonator (Fig. 10.15), under experimental conditions, which correlates to transport rate of nC60 in natural systems. The authors observed no dependence of deposition rate for PLL-coated silica with increasing ionic strength. Rise in deposition rate was reported at higher ionic strengths for HHA-coated silica and bare silica. Charge reverse was probably observed for NaCl solutions higher than 50 mM in all cases. It should be noted that the HHA system had higher deposition rates than PLL and bare silica at all NaCl solutions.

The silica-based system was used to model the release conditions of multiwalled carbon nanotubes (MWCNT) from the surface of soil-like systems using QCM-D [49]. Deposition of MWCNTs on a SiO_2-coated resonator was carried out in the presence of 1.5 mM $CaCl_2$ or 600 nm NaCl, both at pH 7.1. The coated resonator with MWCNT was placed in solutions with different concentrations of NaCl and $CaCl_2$ and pH conditions, corresponding to actual concentrations found in aquatic systems. During the experiments, the change in frequency (ΔF) and dissipation response (ΔD) of the crystal sensors were monitored at different harmonics ($n = 1, 3, 5, 7, 9, 11, 13$). The authors used the Voight-based model, since the values of ΔF and ΔD were significantly different from one another at changing harmonics, and the $\Delta D/\Delta F$ ratio at all harmonics was high (ca. 0.6×10^{-6}/Hz). The results show that MWCNT will be released from the surface at decreasing concentrations of NaCl and $CaCl_2$ solutions and at increasing pH ($pH = 10$). These results are believed to assist in further research of the bioavailability of MWCNTs in the environment as well as for construction of possible water treatment systems.

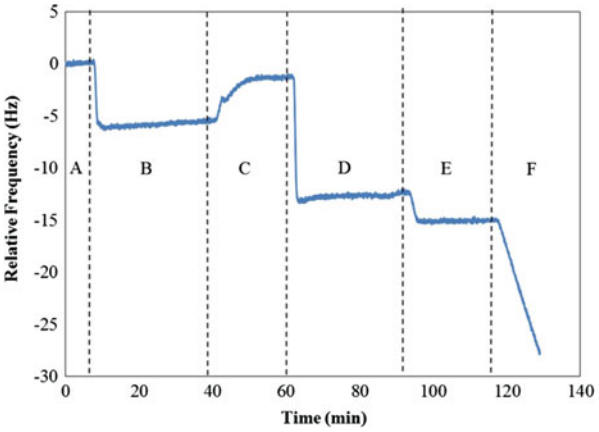

Fig. 10.14 Representative nC60 deposition experiment. The initial baseline was collected in HEPES solution (**a**) before PLL was attached to the silica surface and rinsed in HEPES solution (**b**). The PLL layer was then rinsed in 1 mM NaCl (**c**) before HHA was attached to the PLL surface and rinsed in 1 mM NaCl (**d**). Finally, the HHA layer was rinsed in the electrolyte concentration at which the deposition experiment would take place (100 mM NaCl in this case) (**e**). Once a stable baseline was observed the nC60 was mixed with a premeasured volume of electrolyte to form the desired concentration (100 mM NaCl in this case) and immediately introduced onto the sensor surface (**f**) [48]

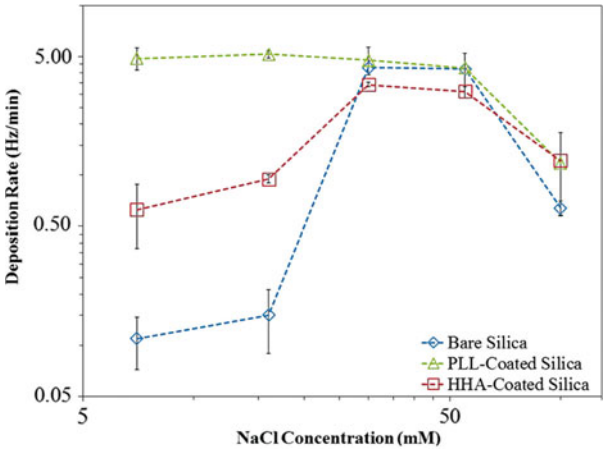

Fig. 10.15 nC60 deposition rates as a function of NaCl concentrations onto three different surfaces [48]

Parallel experiments were carried out for graphene oxide (GO) on the surface of SiO_2 using QCM-D [50]. Changing concentrations of GO were used in the presence of different solutions of NaCl, $CaCl_2$, and $MgCl_2$. A SiO_2-coated QCR was placed in the studied solutions. Measurements were carried out after a lag time of 40 min in order to achieve equilibrium. The deposition attachment efficiency

(α_D) was measured in favorable conditions, achieved by coating the SiO_2 surface with cationic poly-L-lysine hydrobromide. The obtained results for GO deposition in the presence of NaCl and $MgCl_2$ are very similar. These observations fitted the Derjaguin−Landau−Verwey−Overbeek (DLVO) theory, correlating the decreasing deposition rate of GO in high ionic strength conditions. The critical deposition concentration (CDC) for GO exceeds the CDC of carbon nanotubes and fullerenes, showed in prior studies [51, 52]. In the presence of Ca^{2+} ions, GO deposition was negligible, due to the reversible role of Ca^{2+} in the formation of bridges with GO. The release of GO was significantly influenced by the presence of different ions in the solution with an overall trend of NaCl > $MgCl_2$ > $CaCl_2$. In a further research effort, the authors studied the interactions of GO and Al_2O_3 surface in the presence natural organic matter (NOM) [53]. The chosen NOMs were Suwannee River humic and fulvic acids (SRHA and SRFA) and alginate. The experimental method is described above for SiO_2 [50]. The attachment trend of GO to the studied surfaces in a decreasing order was reported as follows: SRFA, SRHA, and aluminum oxide surfaces. The increasing interaction of GO with NOM was attributed to hydroxyl, epoxy, and carboxyl functional groups of GO. In solutions of monovalent and bivalent ions, Na^+ and Ca^{2+}, with concentrations of 10 mM and 1 mM (typical concentrations in aquatic environments), respectively, the rates of deposition of GO on NOM were significantly higher than on Al_2O_3. The authors note that the deposition of GO on NOM and on alumina are highly reversible and, therefore, do not immobilize the distribution of GO in natural aquatic environment.

Following the research of the fate and transport of GO in natural aquatic environmental systems, where the stability of GO against aggregation and deposition was demonstrated, the same authors investigated the possibility of GO transformations and alteration of its properties due to the effect of sunlight [54], since sunlight photolysis is one of the primary routes by which carbonaceous nanomaterials react in natural waters [55, 56]. Moreover, natural organic matter (NOM) can facilitate radical formation under sunlight which can further react with graphene nanomaterials.

Suwannee River humic acid (SRHA) was used as a model NOM. The study was carried out with QCM-D on quartz resonators coated with either clean SiO_2 or with additionally applied SRHA. GO was irradiated with sunlight, prior to any measurements, at different durations (1–187 h) in an/aerobic conditions. The results suggest that on the one hand, photo-induced transformations of GO had slower deposition rate in the presence of NOM and on the other hand, these interactions with NOM were irreversible and no solvation of photo-induced transformations of GO back into water was observed (Fig. 10.16a). It should be noted that photo-induced transformations of GO are faster in anaerobic conditions and therefore have lower mobility in aquatic environments (Fig. 10.16b). The results of this study can be very useful in designing water treatment systems based on irradiation with sunlight or UV.

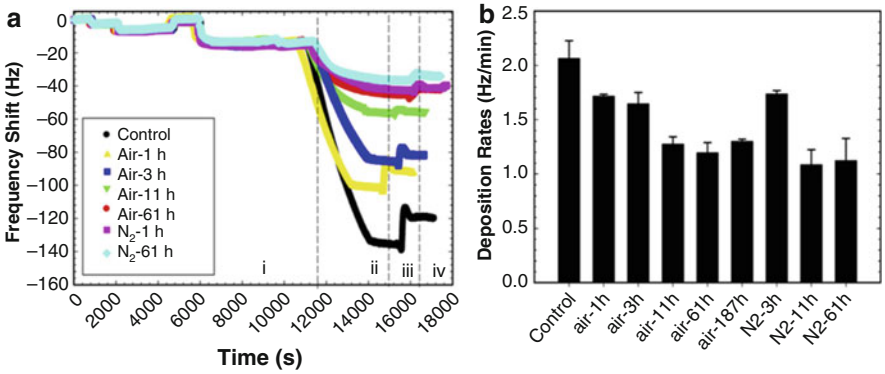

Fig. 10.16 (**a**) Deposition of phototransformed GO on SRHA-coated surface using QCM-D in 30mM NaCl. (A) Frequency shift at the third overtone (Df3) and (**b**) initial deposition rates. Step i: formation of SRHA layer on silica surface; Step ii: injection of phototransformed GO; Step iii: injection of background electrolyte; and Step iv: injection of DI water. GO concentration was maintained 1 mg/L TOC at pH 5.5 ± 0.3 [54]

5.4 Using QCM for Studying of Nanoparticles Deposition and Growth Process

QCM as an in situ tool continues to be one of the most useful and common methods for mass-metric control. QCM is easy to use and can be utilized to study many different processes. The high sensitivity to changes in mass makes this method irreplaceable for investigation of deposition of nanomaterial, their hetero-phasic growth, catalysis on nanoparticles, and finally for processes of modification of nanostructures. The classical application of QCM as a mass-metric device for the study of propagation of different processes continues in recent research.

5.4.1 Application of QCM for Studying Nanostructure Deposition and Interactions with Other Materials

It is well known that the many nanoparticle properties, such as catalytic [57], structural [58], electromagnetic [59, 60], and more, are size dependent. Moreover, the size was shown to effect surface charge properties and due to high surface area and curvature effect of nanoparticles [61–63].

In a recent study, the surface chemistry interactions with a flat SiO_2 surface (curvature ~0) were investigated for three different-sized SiO_2 nanoparticles using QCM-D [64]. Various suspensions of NaCl were used to induce different ionic strengths. The authors monitored the mass changes due to nanoparticle adsorption onto the surface of the quartz resonator, which was coated with a 50 nm layer of SiO_2. The results show that the adsorption of nanoparticles is reduced with the decrease in ionic strength. Almost no adsorption was detected for a solution of 1 mM.

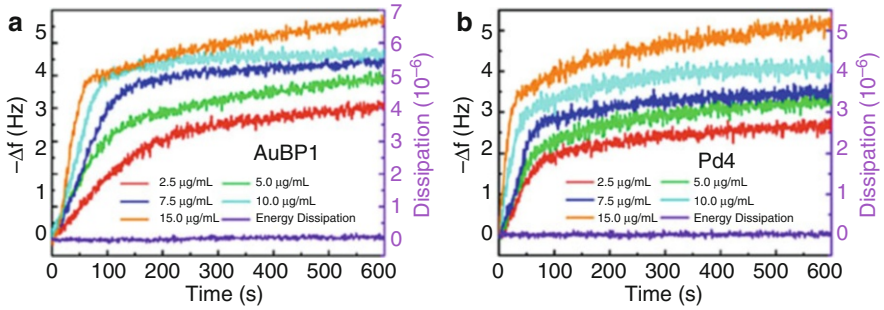

Fig. 10.17 QCM analysis of peptides (**a**) AuBP1 (strongest binder) and (**b**) Pd4 (weakest binder) to obtain ka and kd values [65]

Noncovalent interactions between peptides and gold nanoparticles were investigated using a QCM device, as part of a bionanocombinatorics study, aiming to control the arrangement of the nanocomponents using biomolecules [65].

A standard QCR with a gold electrode was immersed in water solutions of peptides. The authors suggest that equilibrium in the system gold-peptide is achieved after 600 s. The absence of change in dissipation, during these experiments, indicates the presence of a monolayer of peptides on gold, rather than a multilayer (Fig. 10.17). The authors therefore suggest that in such a system, the only favorable interactions are peptide-gold. The change in frequency can be used to characterize the binding interaction between the peptides and the gold nanoparticles and calculate the Gibbs free energy for this interaction.

Unfortunately, the authors do not show the characteristics of the gold electrode, hence it is unclear whether the electrode is composed of nanocrystal gold. The absence of specifications of the gold (particle size, shape, functional groups, etc.) impedes the transfer of the suggested model to other metal particle-peptide systems, even for other gold nanoparticles with other characteristics.

In a recent research effort, QCM was used to monitor mass changes and kinetics of electroless copper deposition (ECD), catalyzed with silver (Ag) nanocubes enclosed by (1 0 0) planes and nanoparticles [66]. The catalyst was applied on the surface of the gold electrode of a QCR. The received electrodes were used for electrochemical deposition of copper. The changes in frequency with time showed that the deposition of copper begins after an incubation period of up to 65 s in the presence of silver (Fig. 10.18). Ag nanoparticles induce a faster deposition than the compared Ag nanocubes.

Silver nanoparticles were used as well to study the silver leaching kinetics from a polysulfone membrane embedded with silver nanoparticles using QCM-D [67]. The nanocomposite solution was applied onto a gold QCR electrode using spin-coating and dried in a desiccator. The authors show the decrease in silver leaching rate with time (Fig. 10.19).

In an attempt to increase the redox activity of carbon electrodes, electrochemical quartz microbalance (EQCM) was used to study the modification process of

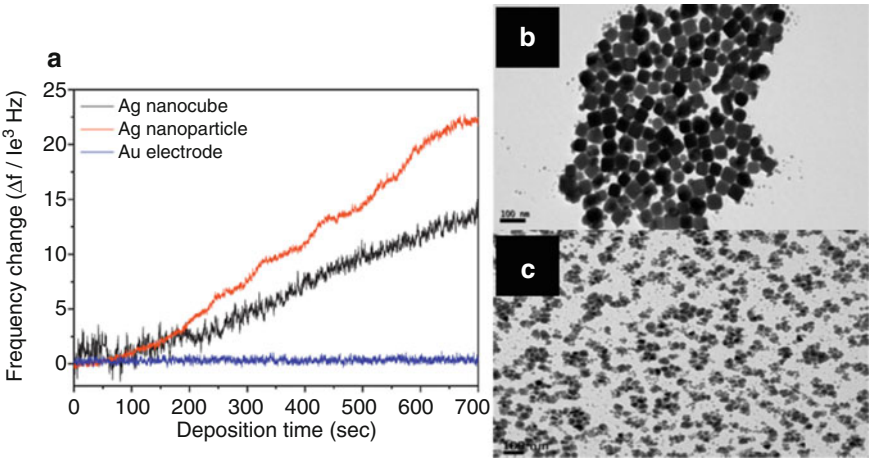

Fig. 10.18 (**a**) Comparison of QCM curves of ECD kinetics in terms of frequency change catalyzed by Ag nanocubes, nanoparticles, and Au electrode, TEM images of Ag catalysts: (**b**) nanocubes and (**c**) nanoparticles [66]

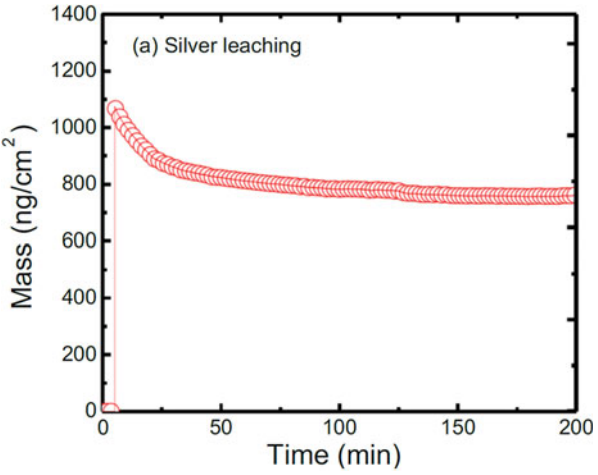

Fig. 10.19 QCM-D measurements of silver leaching from the nanocomposite membrane [67]

multiwalled carbon nanotubes (MWCNT) with quinoline quinones (QLO) for glassy carbon electrodes [68]. The authors suggest a method to obtain highly redox active and stable QLO functionalized MWCNT modified glassy carbon electrode (GCE/MWCNT@QLO) by oxidizing 8-hydroxyquinoline (QL) on GCE/MWCNT. The amount of immobilized QLO on the surface of the MWCNT was determined in situ using EQCM. Changes in mass (Δm) were detected during the process of electrical oxidation in a QL solution when MWCNT modified EQCM-Au electrode (EQCM-Au/MWCNT) was used. The registered amount of passed charge (Q) and Δm allowed the calculation of the molar mass of different intermediate species

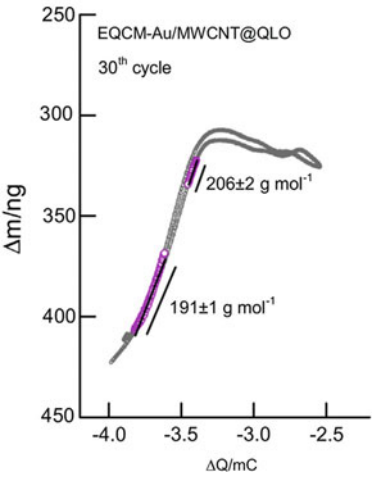

Fig. 10.20 Plot of Δm vs. Q of EQCM-Au/MWCNT@QLO [68]

involved in the electrochemical reactions from the slopes in Fig. 10.20. This method can be useful to study reaction mechanism.

QCM-D was applied for the study of formation of magnetic nanoparticle-vesicle aggregates (MNPVs) as part of the research of transport of proteins and enzymes through phospholipid bilayers via induced magnetic fields [69].

QCM-D confirms the formation of MNPVs when mixing avidin-coated biotinylated APTES ((3-aminopropyl)triethoxysilane)–MNPs and dipalmitoyl phosphatidylcholine vesicles. The authors show that a magnetic impulse can cause the release of proteins and enzymes from within the MNPV into the suspension.

5.4.2 Using QCM for Studying Shape Transformations of Nanostructured Systems

A recent study by Kasputis et al. [70] investigates the formation of new functional nanomaterial through combining organic polymer brushes with gold or silicon slanted columnar thin films (SCTFs) to give unique material properties with potential for applications in chemical and biological sensing, biomaterials, tissue engineering, and nanoelectronics. In situ combinatorial generalized ellipsometry and quartz crystal microbalance with dissipation (GE/QCM-D) were used to demonstrate feasibility of the suggested nanomaterials. The nanomaterial received on the surface of the QCR was shown to swell and deswell under various pH values (Fig. 10.21). These allow to control the geometry of the nanomaterial.

Similar shape transformations as well as changes in viscoelastic properties were induced for Cowpea chlorotic mottle virus (CCMV), used as an active nanomaterial [71]. For this purpose, deposition of CCMVs was carried out on the surface of a gold electrode of a QCR. The change of CCMVs from closed to swollen forms was induced by changing the solution buffer composition. The change in dissipation was the most sensitive parameter to indicate closed and swollen forms due to changes in the viscoelastic properties (Fig. 10.22).

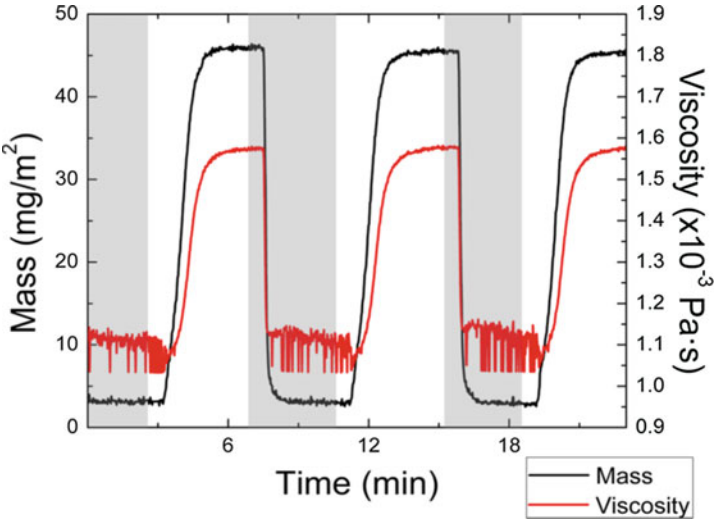

Fig. 10.21 Modeled QCM-D frequency and dissipation data demonstrate the functional swelling characteristics of polymer brushes within SCTFs by changing the pH of the liquid ambient—buffered acetate solution. Changes in pH are indicated by the different shaded background regions on the plots, and changes in pH caused changes in the overall mass (black line) and viscosity (red line) of the thin film, indicative of polymer brush swelling at pH = 7.3 (white background regions) and deswelling at pH = 3.7 (gray-shaded background region) [70]

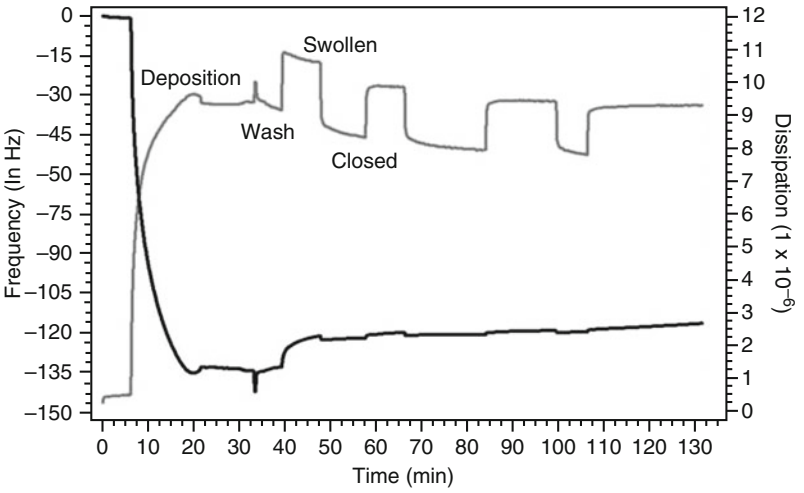

Fig. 10.22 QCM-D analysis of CCMV. Trace shows the frequency (in black, on Y1 axis) and dissipation values (in gray, on Y2 axis) of the third overtone beginning with surface loading of a gold-coated crystal through multiple cycles between swollen and closed conformations. The ratio of frequency to dissipation provides information about the solution phase modulus of the material [71]

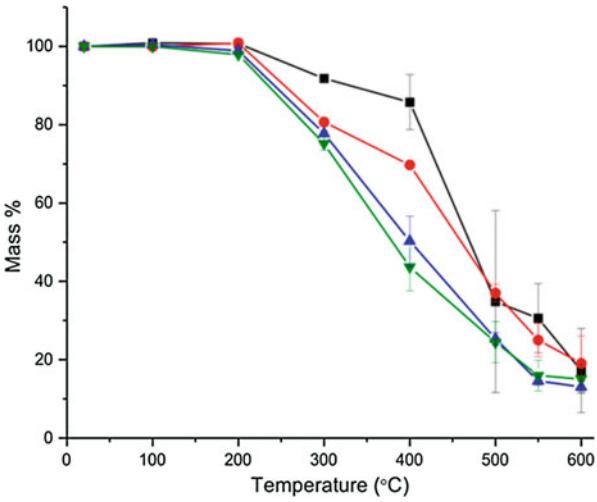

Fig. 10.23 μ-TGA mass % versus temperature thermograms of four layer-by-layer coated Au nanoparticle samples. 30 nm AuNPs + PLL (black), 30 nm AuNPs + PLL + DNA (red), 30 nm AuNPs + PLL + DNA + PLL (blue), and 30 nm AuNPs + PLL + DNA + PLL + DNA (green) [72]

5.4.3 Using QCM for Microscale Thermogravimetric Analysis (μ-TGA)

Mansfield et al. [72] developed the methodology of microscale thermogravimetric analysis (μ-TGA) based on the use of elevated-temperature quartz crystal microbalance. Practically, the authors demonstrate the use of μ-TGA for measurements of nanoparticle purity and presence of any surface coatings of nanomaterials. Samples of nanomaterials in dispersions were applied onto the QCR by drop-cast or by spray-coating. The QCR was then heated for 10 min at 75 °C to remove the water solvent. Layer-by-layer gold nanoparticles (AuNP) were used with a varying number of layers coated by Poly(L-lysine) (PLL) and DNA as well as SiO_2 nanoparticles, coated with polyethylene gycol (SiO_2-PEG) and single-wall carbon nanotubes (SWCNTs). A layer of glass was applied on the QCR prior to carried out experiments with AuNP. μ-TGA was done ex situ: QCR was heated at 10 °C/min to some goal temperature. The QCR was then cooled down and the change in mass registered using QCM. The QCR would then be heated to the next goal temperature up to the desired temperature. A few such cycles were carried out to construct thermogravimetric analysis. Similarly, a QCR with no coatings was heated to the same goal temperatures in order to account for the compensation of the influence of the heating cycles on the quartz crystal. Such compensation is necessary for temperatures above 425°C, where the values of thermal stresses for quartz are not negligible [73].

In addition, mass was recalculated after heating above 100 °C to compensate for the mass of desorbed water. The authors show that their method is sensitive enough to detect mass changes for materials with a difference in one layer for layer-by-layer coated AuNP (Fig. 10.23).

This is by definition an ex situ method; however, the authors are positive that μ-TGA can potentially be used to study nanomaterials in general. This system can involve into an in situ method in condition that the temperature of a QCR could be

changes during the experiment, without the need to interrupt the process. Such a system should also be equipped with a system of signal analysis to compensate for the thermal changes in quartz.

6 Conclusions and Future Perspective

Applying layers of receptor materials on a surface of a QCR is a well-known method that serves as a sensor for detecting various compounds in the gas and liquid phases. In the last decade, these techniques were implemented for nanomaterials, which are used as analytes as well as matrices for applying receptor materials.

Nanomaterials can rarely be used as unique receptor materials for any analyte; hence, nanomaterials can be utilized to assess sensor properties. Important developments in this field are the use of combined methods of research to study complex properties of sensor materials, for instance, QCM and SPM. In this case, QCM can serve as a reliable method of data quantification for integrative properties of a sensor material, which is a complementary data for other specific properties studied by another method.

Researchers who apply layers of receptor materials on QCM to detect nanostructures as analytes experience difficulties similar to the ones described above. The received contradicting results in such cases cannot be used for practical applications. Possible future development in this field can improve the correlations for nanoparticle-receptor interactions and in integration with other methods.

In recent research of nanotoxicology, QCM proved to be more sensitive than other more standard methods. For instance, QCM was reported to be more sensitive to the influence of QDs on the aggregation of human blood platelets than for the commonly used method in such cases, light transmission aggregometry (LTA). The use of QCM to study the influence of nanoparticles on the general and specific bacterial function helped accurately evaluate bacterial secretion functions as well as the decrease in the ability to form biofilms in the presence of TiO_2 nanoparticles. During the study of GO interactions with liposomes, the combined analysis of the change in frequency and dissipation allowed building a possible schematic representation of GO-lipid formation process. This in turn can prove useful for study of environmental aspects of nanomaterials.

Moreover, QCM is a useful tool for the study of nanoparticle interactions with model soil-like materials (alumina, silica) and model DOMs (Suwannee River humic, fulvic acids, Harpeth humic acids, Harpeth fulvic acids), which are essential when assessing processes of distribution, transport, and accumulation of nanomaterials in natural environments. The works presented in this chapter are dedicated primarily to the study of environmental aspects of metal-based nanoparticles: gold nanospheres, gold nanorods, CdTe/CdS and CdSe/ZnS quantum dots, as well as carbon nanoforms: fullerene, carbon nanotubes, and GO. The shift in frequency of QCM can be used to evaluate the deposition rate of nanoparticles in different solution compositions. Based on similar measurements, favorable deposition conditions of nanoparticles can be determined. Such information can prove useful for

predicting the effects of nanostructures on the surrounding environment and for possible water treatment systems.

Many recent works utilized QCM as an in situ tool for mass-metric control of various processes involving nanostructures.

QCM was used to gather essential experimental data to develop general models of noncovalent interactions of nanoparticles with different materials and complexes. Since these papers stand-alone in their line of research and tend to be more exploratory, the presented results in these studies are of a theoretical nature.

The use of the combination of QCM with an electrochemical chamber to study the modification processes of nanotubes allowed determining the composition of intermediate reaction products and to suggest a possible mechanism for the process. This method was validated with techniques such as XPS, FTIR, and GC-MS.

A developed thermogravimetric analysis based on in situ heating of a QCR is of great interest. Unfortunately, this technique was developed for ex situ measurements. If further engineering can solve a line of constructive problems, we could have real-time thermogravimetric resolution.

In the meantime and in the near future, QCM will be utilized for the studies of dependence of material properties as a function of the nanostructure shape in various processes. Moreover, the application of EQCM for the study of electrochemical processes involving nanomaterials can develop in utilizing two QCRs with different electrode materials for simultaneous monitoring of changes in mass on both the electrodes of the electrochemical chamber.

Examples of research progress in the direction of integration of a few analytical methods together can be QCM and IR, as well as the combination of EQCMs. These kinds of study can be proven very useful to investigate nanomaterial sensors and for detection processes of gas analytes.

In conclusion, definite and easily analyzed measurements with QCM can usually be received for the cases of thin rigid films in a gas-filled detection chamber of in vacuum. These kinds of measurements are commonly used for process control in electronics and for study of gas sensors.

The interpretation of QCM measurements for deposition of complex bulky nanostructures, especially deposition from the liquid phase, involves a thorough experiment planning and the use of additional verification methods. The development of the QCM methodology is still in progress. Today QCM can seldom be used as a stand-alone research method; however, as a complementary method, QCM can provide useful and unique information for unfolding processes involving nanomaterials.

Nomenclature

C_m	Constant of the resonator parameters
D	Dissipation factor [−]
F	Resonance frequency [1/T]
F_0	Natural vibration frequency of the QCR [1/T]
h_f	Thickness of film [L]
h_q	Thickness of quartz [L]

n	Number of harmonics [−]
s	Area of oscillation in the QCR [L^2]
ΔD	Change in dissipation [−]
Δf	Change in frequency [1/T]
Δm	Change in mass [M]
η_f	Viscosity of the film [$M \cdot L^{-1} \cdot T^{-1}$]
η_L	Viscosity of liquid [$M \cdot L^{-1} \cdot T^{-1}$]
μ_f	Elastic modulus [$M \cdot L^{-1} \cdot T^{-2}$]
ρ_f	Density of coated film [$M \cdot L^{-3}$]
ρ_L	Density of liquid [$M \cdot L^{-3}$]
ρ_q	Density of quartz [$M \cdot L^{-3}$]
τ	Decay time constant [T]

References

1. Curie J, Curie P (1880) Développement Par Pression de L'électricite Polaire Dans Les Cristaux Hémièdres À Faces Inclinées. Comptes Rendus l'Academie Des Sci 91:294–295
2. Lippman G (1881) Sur Le Principe de La Conservation de L'électricité, Ou Second Principe de La Théorie Des Phénomènes Électriques. Comptes Rendus l'Academie Des Sci. 92:1049–1051
3. Curie J, Curie P (1882) Déformations Électriques Du Quartz. Comptes Rendus l'Académie Des Sci 95:914–917
4. Sauerbrey G (1959) Verwendung von Schvangquarzen Zur Wag-Ung Dunner Schichten Und Zur Mikrowagung. Zeitschrift Fur Phys 155(2):206–222
5. Czanderna AW, Lu C (1984) Applications of Piezoelectric quartz crystal microbalances. In: Lu C, Czanderna AW (eds) Methods phenom, vol 7. Elsevier, Amsterdam, The Netherlands
6. Kim H (2003) Atomic layer deposition of metal and nitride thin films: current research efforts and applications for semiconductor device processing. J Vac Sci Technol B Microelectron Nanometer Struct 21(6):2231
7. Petosa AR, Jaisi DP, Quevedo IR, Elimelech M, Tufenkji N (2010) Aggregation and deposition of engineered nanomaterials in aquatic environments: role of physicochemical interactions. Environ Sci Technol 44(17):6532–6549
8. Wang X, Ding B, Sun G, Wang M, Yu J (2013) Electro-spinning/netting: a strategy for the fabrication of three-dimensional polymer Nano-fiber/nets. Prog Mater Sci 58(8):1173–1243
9. Ding B, Wang M, Wang X, Yu J, Sun G (2010) Electrospun nanomaterials for ultrasensitive sensors. Mater Today 13(11):16–27
10. Radomska A, Leszczyszyn J, Radomski M (2016) The Nanopharmacology and Nano-toxicology of nanomaterials: new opportunities and challenges. Adv Clin Exp Med 25 (1):151–162
11. Li L, Mu Q, Yan B (2010) Analytical strategies for detecting nanoparticle – protein interactions. Analyst 135:1519–1530
12. Ariga K, Yamauchi Y, Ji Q, Yonamine Y, Hill JP (2014) Research update: mesoporous sensor Nanoarchitectonics. APL Mater 2(3):30701
13. Wang L, Sun Y, Li Z, Wu A, Wei G (2016) Bottom-up synthesis and sensor applications of biomimetic nanostructures. Materials (Basel) 9(1):53
14. de la Escosura-Muñiz A, Parolo C, Merkoçi A (2010) Immunosensing using nanoparticles. Mater Today 13(7–8):24–34
15. Cea P, Martín S, González-Orive A, Osorio HM, Quintín P, Herrer L (2016) Nanofabrication and electrochemical characterization of self-assembled monolayers sandwiched between metal nanoparticles and electrode surfaces. J Chem Educ 93(8):1441–1445

16. Hahm J-I (2013) Biomedical detection via macro- and Nano-sensors fabricated with metallic and semiconducting oxides. J Biomed Nanotechnol 9(1):1–25
17. Afzal A, Iqbal N, Mujahid A, Schirhagl R (2013) Advanced vapor recognition materials for selective and fast responsive surface acoustic wave sensors: a review. Anal Chim Acta 787:36–49
18. Bhakta SA, Evans E, Benavidez TE, Garcia CD (2015) Protein adsorption onto nanomaterials for the development of biosensors and analytical devices: a review. Anal Chim Acta 872:7–25
19. Krizkova S, Heger Z, Zalewska M, Moulick A, Adam V, Kizek R (2015) Nanotechnologies in protein microarrays. Nanomedicine 10(17):2743–2755
20. Wark AW, Lee J, Kim S, Faisal SN, Lee HJ (2010) Bioaffinity detection of pathogens on surfaces. J Ind Eng Chem 16(2):169–177
21. Li Z, Yu Y, Li Z, Wu T (2015) A review of biosensing techniques for detection of trace carcinogen contamination in food products. Anal Bioanal Chem 407(10):2711–2726
22. Chen Q, Xu S, Liu Q, Masliyah J, Xu Z (2016) QCM-D Study of nanoparticle interactions. Adv Colloid Interf Sci 233:94–114
23. Höök F, Kasemo B, Nylander T, Fant C, Sott K, Elwing H (2001) Variations in coupled water, viscoelastic properties, and film thickness of a Mefp-1 protein film during adsorption and cross-linking: a quartz crystal microbalance with dissipation monitoring, ellipsometry, and surface plasmon resonance study. Anal Chem 73(24):5796–5804
24. Rodahl M, Kasemo B (1996) On the measurement of thin liquid Overlayers with the quartz-crystal microbalance. Sensors Actuators A Phys 54:448–456
25. Voinova MV, Rodahl M, Jonson M, Kasemo B (1999) Viscoelastic acoustic response of layered polymer films at fluid-solid interfaces: continuum mechanics approach. Phys Scr 59(5):391–396
26. P-G S, Kuo X-R (2014) Low-humidity sensing properties of carboxylic acid functionalized carbon nanomaterials measured by a quartz crystal microbalance. Sensors Actuators A Phys 205:126–132
27. Marrazza G (2014) Piezoelectric biosensors for organophosphate and carbamate pesticides: a review. Biosensors 4(3):301–317
28. Popov VS, Subcheva EN, Shelaev AV, Pavelko RG, Sevastyanov VG, Kuznetsov NT (2014) Scanning probe microscope-quartz crystal microbalances integrated system for in-situ study of sensor properties of microamounts of nanomaterials. Theor Found Chem Eng 48(4):518–523
29. Bykov A, Shelaev A (2008) Scanning probe microscope combined with device for measuring mass and dissipative properties. Patent RU 2407021C2
30. Barsan MM, David M, Florescu M, Ţugulea L, Brett CMA (2014) A new self-assembled layer-by-layer glucose biosensor based on chitosan biopolymer entrapped enzyme with nitrogen doped graphene. Bioelectrochemistry 99:46–52
31. Du X, Jiang D, Hao N, Qian J, Dai L, Zhou L, Hu J, Wang K (2016) Building a three-dimensional Nano–bio Interface for Aptasensing: an analytical methodology based on steric hindrance initiated signal amplification effect. Anal Chem 88(19):9622–9629
32. McWilliams A (2014) Nanotechnology: a realistic market assessment. BCC Research, Wellesley, MA
33. Jang K, You J, Park C, Park H, Choi J, Choi C-H, Park J, Lee H, Na S (2016) Ultra-sensitive detection of zinc oxide nanowires using a quartz crystal microbalance and phosphoric acid DNA. Nanotechnology 27(36):365501
34. Jang K, Park C, You J, Choi J, Park H, Park J, Lee H, Choi C-H, Na S (2016) Highly sensitive, direct and real-time detection of silver nanowires by using a quartz crystal microbalance. Nanotechnology 27(47):475506
35. Jang K, Park J, Lee S, You J, Park C, Lee J, Park W, Yun J, Ahn S, Na S (2015) Situ and fast detection of single-walled carbon nanotubes by using DNA mediated aggregation method and quartz crystal microbalance. J Appl Phys 118(3):34510

36. Dobrovolskaia MA, Aggarwal P, Hall JB, McNeil SE (2008) Preclinical studies to understand nanoparticle interaction with the immune system and its potential effects on nanoparticle biodistribution. Mol Pharm 5(4):487–495
37. Prina-Mello A, Samuel S, Medina C, Jain N, Radomski M, Volkov Y, Santos-Martinez M (2015) CdTe quantum dots induce activation of human platelets: implications for nanoparticle Hemocompatibility. Int J Nanomedicine 10:2723
38. Wang J, Cao Y, Li Q, Liu L, Dong M (2015) Size effect of graphene oxide on modulating amyloid peptide assembly. Chem A Eur J 21(27):9632–9637
39. Yi P, Chen KL (2013) Interaction of multiwalled carbon nanotubes with supported lipid bilayers and vesicles as model biological membranes. Environ Sci Technol 47(11):5711–5719
40. Richter RP, Lai Kee Him J, Tessier B, Tessier C, Brisson AR (2005) On the kinetics of adsorption and two-dimensional self-assembly of Annexin A5 on supported lipid bilayers. Biophys J 89(5):3372–3385
41. Frost R, Svedhem S, Langhammer C, Kasemo B (2016) Graphene oxide and lipid membranes: size-dependent interactions. Langmuir 32(11):2708–2717
42. Westas E, Svanborg LM, Wallin P, Bauer B, Ericson MB, Wennerberg A, Mustafa K, Andersson M (2015) Using QCM-D to study the adhesion of human gingival fibroblasts on implant surfaces. J Biomed Mater Res Part A 103(10):3139–3147
43. Maurer-Jones MA, Gunsolus IL, Meyer BM, Christenson CJ, Haynes CL (2013) Impact of TiO 2 nanoparticles on growth, biofilm formation, and Flavin secretion in Shewanella Oneidensis. Anal Chem 85(12):5810–5818
44. Afrooz ARMN, Sivalapalan ST, Murphy CJ, Hussain SM, Schlager JJ, Saleh NB (2013) Spheres vs. rods: the shape of gold nanoparticles influences aggregation and deposition behavior. Chemosphere 91(1):93–98
45. Quevedo IR, Olsson ALJ, Tufenkji N (2013) Deposition kinetics of quantum dots and polystyrene latex nanoparticles onto alumina: role of water chemistry and particle coating. Environ Sci Technol 47(5):2212–2220
46. Tong M, Ding J, Shen Y, Zhu P (2010) Influence of biofilm on the transport of fullerene (C60) nanoparticles in porous media. Water Res 44(4):1094–1103
47. McNew CP, LeBoeuf EJ (2015) The role of attached phase soil and sediment organic matter physicochemical properties on fullerene (nC60) attachment. Chemosphere 139:609–616
48. McNew CP, LeBoeuf EJ (2016) nC60 deposition kinetics: the complex contribution of humic acid, ion concentration, and valence. J Colloid Interface Sci 473:132–140
49. Yi P, Chen KL (2013) Influence of solution chemistry on the release of multiwalled carbon nanotubes from silica surfaces. Environ Sci Technol 47(21):12211–12218
50. Chowdhury I, Duch MC, Mansukhani ND, Hersam MC, Bouchard D (2014) Deposition and release of graphene oxide nanomaterials using a quartz crystal microbalance. Environ Sci Technol 48(2):961–969
51. Chang X, Bouchard DC (2013) Multiwalled carbon nanotube deposition on model environmental surfaces. Environ Sci Technol 47(18):10372–10380
52. Chen KL, Elimelech M (2008) Interaction of fullerene (C 60) nanoparticles with humic acid and alginate coated silica surfaces: measurements, mechanisms, and environmental implications. Environ Sci Technol 42(20):7607–7614
53. Chowdhury I, Duch MC, Mansukhani ND, Hersam MC, Bouchard D (2014) Interactions of graphene oxide nanomaterials with natural organic matter and metal oxide surfaces. Environ Sci Technol 48(16):9382–9390
54. Chowdhury I, Hou W-C, Goodwin D, Henderson M, Zepp RG, Bouchard D (2015) Sunlight affects aggregation and deposition of graphene oxide in the aquatic environment. Water Res 78:37–46
55. Cheng Y, Yin L, Lin S, Wiesner M, Bernhardt E, Liu J (2011) Toxicity reduction of polymer-stabilized silver nanoparticles by sunlight. J Phys Chem C 115(11):4425–4432
56. Hou W-C, Chowdhury I, Goodwin DG, Henderson WM, Fairbrother DH, Bouchard D, Zepp RG (2015) Photochemical transformation of graphene oxide in sunlight. Environ Sci Technol 49(6):3435–3443

57. Cuenya BR (2010) Synthesis and catalytic properties of metal nanoparticles: size, shape, support, composition, and oxidation state effects. Thin Solid Films 518(12):3127–3150
58. Chen X, Mao SS (2007) Titanium dioxide nanomaterials: synthesis, properties, modifications, and applications. Chem Rev 107(7):2891–2959
59. Lu L, Li L, Wang X, Li G (2005) Understanding of the finite size effects on lattice vibrations and electronic transitions of. J Phys Chem B 109:17151–17156
60. Woldu T, Raneesh B, Reddy MVR, Kalarikkal N (2016) Grain size dependent Magnetoelectric coupling of BaTiO 3 nanoparticles. RSC Adv 6(10):7886–7892
61. Abbas Z, Labbez C, Nordholm S, Ahlberg E (2008) Size-dependent surface charging of nanoparticles. J Phys Chem C 112(15):5715–5723
62. Holmberg JP, Ahlberg E, Bergenholtz J, Hassellöv M, Abbas Z (2013) Surface charge and interfacial potential of titanium dioxide nanoparticles: experimental and theoretical investigations. J Colloid Interface Sci 407:168–176
63. Barisik M, Atalay S, Beskok A, Qian S (2014) Size dependent surface charge properties of silica nanoparticles. J Phys Chem C 118(4):1836–1842
64. Seo J, Kim JH, Lee M, Moon J, Yi DK, Paik U (2016) Size-dependent interactions of silica nanoparticles with a flat silica surface. J Colloid Interface Sci 483:177–184
65. Tang Z, Palafox-Hernandez JP, Law W-C, Hughes ZE, Swihart MT, Prasad PN, Knecht MR, Walsh TR (2013) Biomolecular recognition principles for Bionanocombinatorics: an integrated approach to elucidate Enthalpic and entropic factors. ACS Nano 7(11):9632–9646
66. Lee C-L, Tsai Y-L, Chen C-W (2013) Specific and mass activity of silver Nanocube and nanoparticle-based catalysts for electroless copper deposition. Electrochim Acta 104:185–190
67. Liu Y, Rosenfield E, Hu M, Mi B (2013) Direct observation of bacterial deposition on and detachment from nanocomposite membranes embedded with silver nanoparticles. Water Res 47 (9):2949–2958
68. Swetha P, Devi KSS, Kumar AS (2014) In-situ trapping and confining of highly redox active quinoline quinones on MWCNT modified glassy carbon electrode and its selective electrocatalytic oxidation and sensing of hydrazine. Electrochim Acta 147:62–72
69. Booth A, Pintre IC, Lin Y, Gough JE, Webb SJ (2015) Release of proteins and enzymes from vesicular compartments by alternating magnetic fields. Phys Chem Chem Phys 17 (24):15579–15588
70. Kasputis T, Koenig M, Schmidt D, Sekora D, Rodenhausen KB, Eichhorn K-J, Uhlmann P, Schubert E, Pannier AK, Schubert M, Stamm M (2013) Slanted columnar thin films prepared by glancing angle deposition functionalized with Polyacrylic acid polymer brushes. J Phys Chem C 117(27):13971–13980
71. Rayaprolu V, Manning BM, Douglas T, Bothner B (2010) Virus particles as active nanomaterials that can rapidly change their viscoelastic properties in response to dilute solutions. Soft Matter 6(21):5286–5288
72. Mansfield E, Tyner KM, Poling CM, Blacklock JL (2014) Determination of nanoparticle surface coatings and nanoparticle purity using microscale thermogravimetric analysis. Anal Chem 86(3):1478–1484
73. Mansfield E, Kar A, Quinn TP, Hooker SA (2010) Quartz crystal microbalances for microscale thermogravimetric analysis. Anal Chem 82(24):9977–9982